EXPERIMENTAL PROCEDURES

Cell Culture—HCT116 cells and HEK293T cells were maintained in low glucose Dulbecco's modified Eagle's medium (Nacalai Tesque, Kyoto, Japan) supplemented with 10% fetal bovine serum (BioWest, Nuaillé, France), and 100 units of penicillin/streptomycin.

Mice—Construction of *Lkb1* knock-out mice has been described previously (10). We only used males due to the low incidence of nodular foci and HCCs in female *Lkb1*(+/−) mice, as reported previously. All animal experiments were approved by the Animal Care and Use Committee of Kyoto University.

Reagents—A mouse monoclonal anti-LKB1 (clone Ley37D/G6), anti-Myc (clone 9E10) and rabbit polyclonal anti-PAK1 antibodies were purchased from Santa Cruz Biotechnology (Santa Cruz, CA). Rabbit polyclonal anti-phospho-PAK1 (Ser^{144})/PAK2 (Ser^{141}), anti-phospho-PAK1 ($Ser^{199/204}$)/PAK2 (Ser^{201}), anti-PAK1 and anti-phospho-Vasodilator-stimulated phosphoprotein (VASP) (Ser^{239}) antibodies were from Cell Signaling Technology (Danvers, MA), and rabbit polyclonal anti-VASP antibody was from EMD Chemicals (Gibbstown, NJ). A mouse monoclonal anti-β-actin antibody was from Sigma-Aldrich (St. Louis, MO), and a mouse monoclonal anti-Hemagglutinin antibody was from Invivogen (San Diego, CA). Two different small interfering RNAs against human LKB1, and scramble siRNA pools were purchased from Dharmacon, Inc. (Lafayette, CO).

cDNA—The following cDNAs were isolated by standard PCR-based cloning techniques: human LKB1, NCBI accession no. NM_000455 and human STRAD, respectively, NCBI accession no. NM_001003787. HA and FLAG tags were attached to the N termini of LKB1 and STRAD, as described previously (17). LKB1 (kinase-dead, a catalytically inactive version of LKB1 with a D194A mutation (30)), was generated with QuikChange II site-directed mutagenesis kit (Stratagene, La Jolla, CA) according to the manufacturer's protocol. Wild-type of PAK1, constitutively active mutant T423E, and a dominant-negative mutant H83LH86LK299R were kindly gifted by Dr. Jonathan Chernoff (Fox Chase Cancer Center). Appropriate PCR primers were used to generate the point mutants PAK1-T109E and PAK1-T109A with the QuikChange II site-directed mutagenesis kit. These BamHI/EcoRI fragments were subcloned into pCMV-Tag 3B (Stratagene), which has an N-terminal Myc tag and a cytomegalovirus promoter.

PAK1-K299R Lentivirus—The NotI/SalI fragment of pCMV-Tag3B-PAK1-K299R was subcloned into pLEX vector (Open Biosystems, Huntsville, AL). Recombinant lentivirus encoding K299R was prepared according to the manufacturer's protocol.

Establishment of an Lkb1-null Mouse Embryonic Fibroblast (MEF) Cell Line—*Lkb1*(+/−) mice (C57BL/6N background) were crossed with outbred ICR mice, and offspring were intercrossed. *Lkb1*-null embryos at 9.5 days post-coitum were minced, trypsinized briefly, and placed on 24-well plates. These cells were cultured in RPMI 1640 (Sigma) with 10% (v/v) fetal bovine serum and 50% (v/v) conditioned medium from the MEFs that were derived from wild-type embryos at 12.5 days post-coitum. We obtained a spontaneously immortalized cell line (MEF3) by continuous passages (>3 months) of the *Lkb1*-null MEFs and further established the subclone MEF3-2 cell line. Finally, we cultured MEF3-2 in Dulbecco's modified Eagle's medium (Sigma) with 10% (v/v) fetal bovine serum.

Recombinant Adenoviruses—Recombinant adenoviruses were constructed by Adeno-X expression system 1 (Clontech Laboratories, Mountain View, CA), according to the manufacturer's protocol. The titers of the recombinant adenoviruses were determined by the method previously reported by others (31).

Wound-healing Assay—Cells were infected with recombinant adenovirus; after 24 h of infection, wounds were incised by scratching the cell monolayer using 10-μl pipette tips. Photographs were taken at 0 and 20 h after the wound was made. Cell migration was normalized so that 100% represents the migration distance of control cells.

Transfection—HEK293T cells were transfected with plasmid DNA of the indicated PAK1 and LKB1 expression vectors using Lipofectamine 2000 (Invitrogen). After 24 h of transfection, cell lysates were prepared for Western blotting or *in vitro* kinase assay. Lipofectamine 2000 RNAiMAX (Invitrogen) was used for small interfering RNA (siRNA) transfection according to manufacturer's protocol.

Recombinant PAK1 Proteins Produced in Escherichia coli—PAK1-PBD was isolated by standard PCR-based cloning techniques. The PAK1-PBD-T109A mutant was generated with the QuikChange II site-directed mutagenesis kit. To attach GST protein to PAK1-PBD, PAK1-PBD-T109A, PAK1-K299R, or PAK1-T109A/K299R was inserted in the BamHI-double digested pGEX-6P-1 vector (GE Healthcare). pGEX-2TK-VASP-(158–277) was generated previously (32). 200 ml of 2×YT medium (1.6% tryptone, 1% yeast extract, and 0.5% NaCl) medium was inoculated with *E. coli* (BL21 strain) containing the recombinant pGEX-2TK plasmid that encodes GST-VASP-(158–277), or the recombinant pGEX-6P-1 plasmid that encodes GST-PAK1-PBD, GST-PAK1-PBD-T109A, GST-PAK1-K299R, or GST-PAK1-T109A/K299R and was incubated at 37 °C in the presence of 100 μg/ml ampicillin until A_{600} reached 0.8. To induce expression of the GST-tagged proteins, isopropyl-D-thiogalactopyranoside was added at 100 μM. After culture for 24 additional hours at 25 °C, cells were harvested, and recombinant proteins were purified as described previously (17).

Western Blotting—Cells were lysed in the lysis buffer (50 mM Tris-HCl (pH 7.4), 150 mM NaCl, 5 mM $Na_4P_2O_7$, 10 mM β-glycerophosphate, 25 mM NaF, 1 mM EDTA, 1 mM EGTA, 1 mM Na_3VO_4, and 1% (v/v) Triton X-100) containing Complete mini protease inhibitor mixture (Roche Applied Science). Cell lysates were separated by SDS-PAGE and transferred to Immobilon-P membrane (Millipore, Billerica, MA). After blocking with Blocking One or Blocking One-P (Nacalai Tesque, Kyoto, Japan), the membranes were probed with the indicated antibodies. The signals were visualized by Immobilon western detection system (Millipore) or ECL Western blotting detection reagents (GE Healthcare).

In Vitro Phosphorylation Assay—Phosphorylation reactions were performed at 30 °C in the phosphorylation reaction buffer (50 mM Tris-HCl (pH 7.0), 10 mM $MgCl_2$, 2 mM $MnCl_2$, 5 mM β-glycerophosphate, 100 μM Na_3VO_4, 1 mM dithiothreitol, and

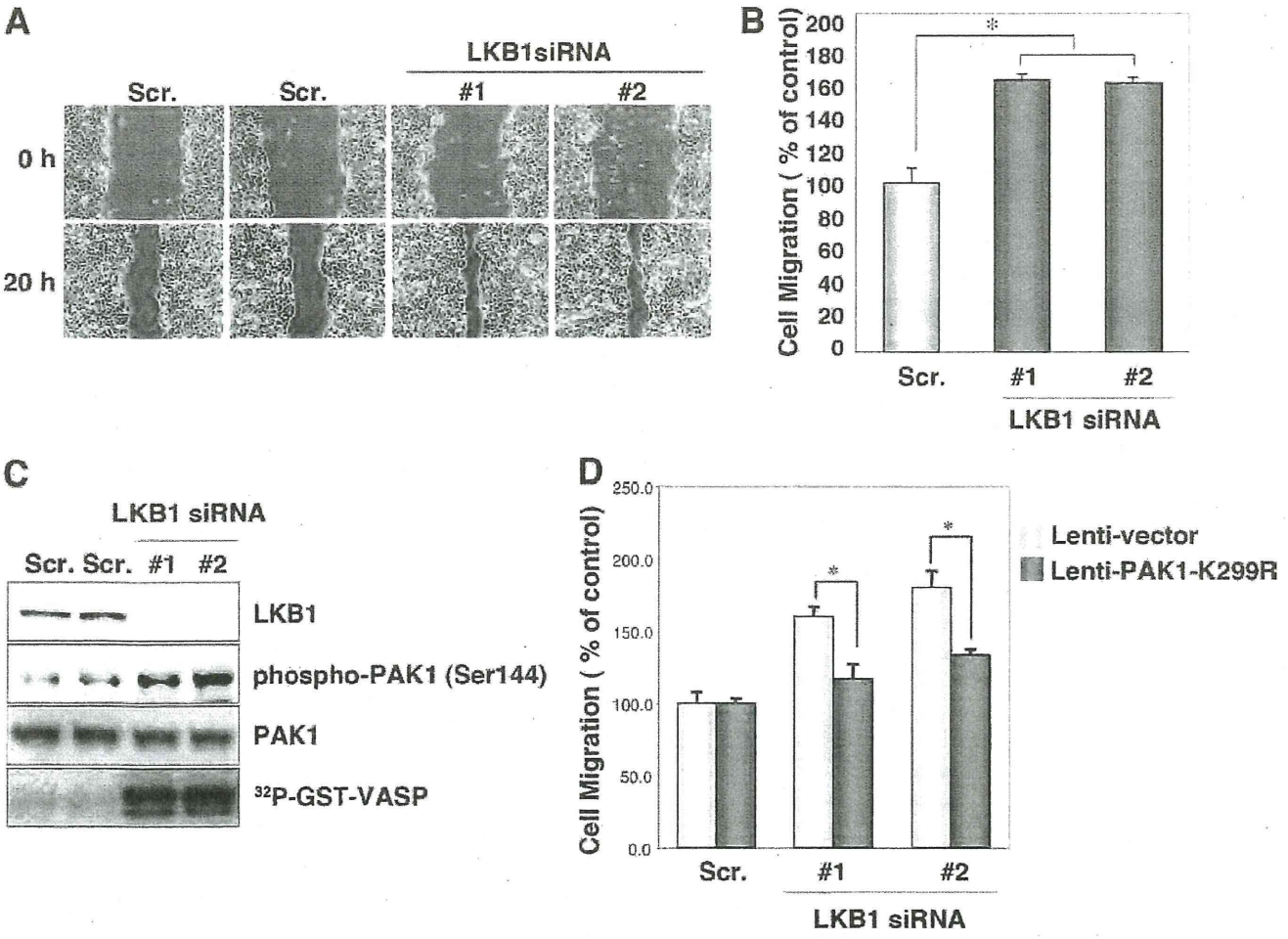

FIGURE 1. **Knockdown of endogenous LKB1 increases cell migration and PAK1 activity in HCT116 cells.** *A*, knockdown of LKB1 increases cell migration. HCT116 cells were transfected with two different specific siRNAs against human LKB1. Control cells were transfected with a scrambled (*Scr.*) siRNA pool. After 24 h of plating, scratches were made with 10-μl pipette tips. Photographs were taken at 0 and 20 h after the wound was made. *B*, cell migration was normalized so that 100% represented migration distance of control cells. *Error bars* indicate S.D. The *asterisk* indicates significant increases compared with control cells ($p < 0.001$). *C*, cellular levels of phospho-PAK1 (Ser^{144}), total PAK1 and *in vitro* PAK1 activity in LKB1 knockdown HCT116 cells. Lysates were prepared from HCT116 cells transfected with the indicated siRNAs. The levels of phospho-PAK1 (Ser^{144}) and PAK1 were determined by Western blotting with the indicated antibodies. Lysates were prepared from HCT116 cells transfected with the indicated siRNAs and immunoprecipitated using an anti-PAK1 antibody. The precipitates were used for *in vitro* kinase assays using GST-VASP-(158–277) as a substrate. The phosphorylation of GST-VASP was visualized using BAS-5000 Bio-imaging Analyzer. *D*, induction of PAK1-K299R suppressed the increase in migration in LKB1 knockdown cells. The cells transfected with the indicated siRNAs were then infected with lentivirus lenti-PAK1-K299R or lenti-vector. At 24 h post-infection, cultures were scratches were made with 10-μl pipette tips. Photographs were taken at 0 and 20 h thereafter. Cell migration was normalized so that 100% represented the migration distance of control cells. *Error bars* indicate S.D. The *asterisk* represents significant increases compared with control cells ($p < 0.001$).

200 μM ATP). As shown in Figs. 1*C* and 2*B*, the immunoprecipitates obtained from cell lysates using anti-PAK1 antibody were incubated with GST-VASP-(158–277) for 20 min. The reactions were stopped by the addition of 3× sample buffer (150 mM Tris-HCl (pH 6.8), 6% (w/v) SDS, 0.03% (w/v) bromphenol blue, 30% (v/v) glycerol, and 15% (v/v) 2-mercaptoethanol). The anti-Myc immunoprecipitates from HEK293T cell lysates were incubated with 5 μg of GST-VASP-(158–277) for 20 min with [γ-^{32}P]-ATP (see Figs. 3*A* and 5). The reactions were then terminated by the addition of 3× sample buffer. The samples were electrophoresed on 5–20% SDS-PAGE gels. The blots were exposed to a phosphor imaging plate (Fujifilm, Tokyo, Japan). The signals were detected by using BAS-5000 Bio-imaging Analyzer (Fujifilm). All assays using [γ-^{32}P]ATP were done at the Radioisotope Research Center of Kyoto University. Fold induction was determined using NIH Image (version 1.62). Recombinant LKB1/STRAD/MO25 (Millipore) was preincubated with recombinant PAK1 (EMD Chemicals) in the presence of ATP for 20 min, and then the reaction mixtures were incubated with 5 μg of GST-VASP-(158–277) for 20 min (see Fig. 3*B*). The cellular levels of phosphorylated VASP were detected using an anti-phospho-VASP (Ser^{239}) antibody.

Statistical Analysis—Results of the experimental studies were reported as mean ± S.D. Differences were analyzed by Student's *t* test. A value of $p < 0.05$ was regarded as significant.

RESULTS

Knockdown of Endogenous LKB1 Enhances Cell Migration and PAK1 Activity in HCT116 Cells—We have reported previously that HCCs in *Lkb1*(+/−) mice metastasize to the lungs (10). Consistently, LKB1 also appears to suppress lung cancer metastasis (33). To investigate the mechanism(s) by which

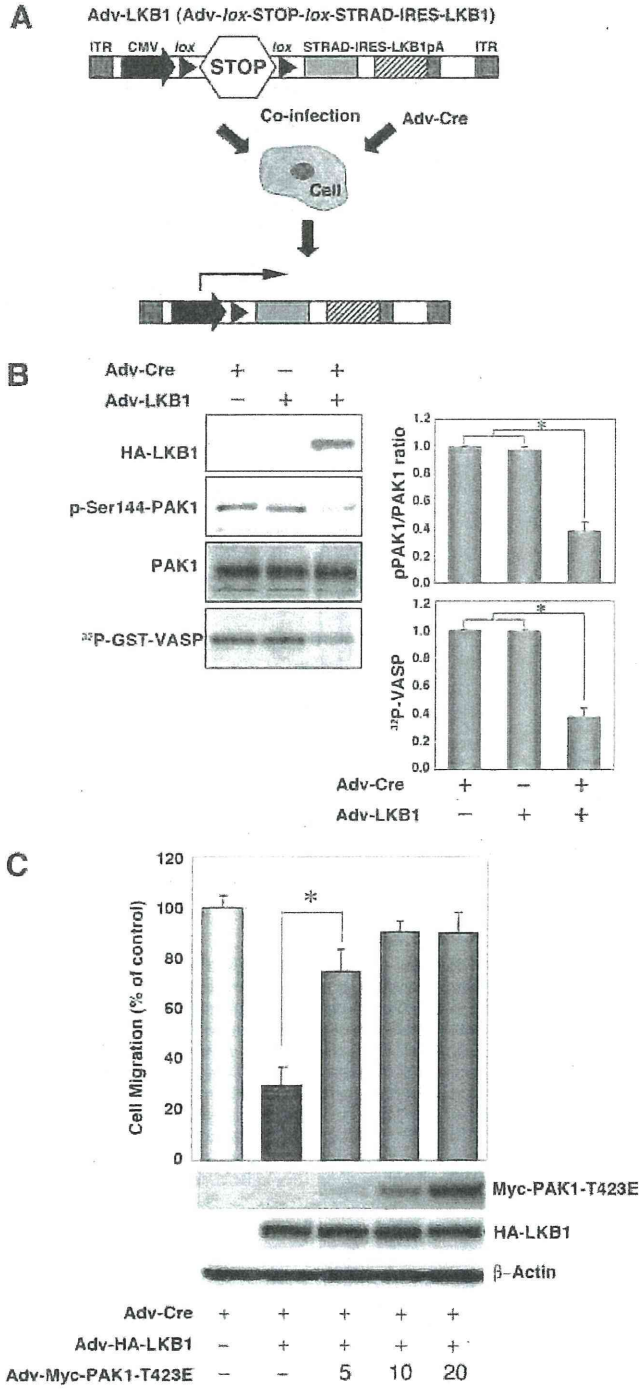

FIGURE 2. **Expression of LKB1 in the *Lkb1*-null MEF cell line (MEF3-2) inhibits cell migration and PAK1 activation.** *A*, schematic structure of the adenoviral construct, adapted from Ref. 17. *ITR*, inverted terminal repeat; *CMV*, human cytomegalovirus immediate early promoter; *lox*, loxP site sequence; *STOP*; transcriptional termination cassette; *IRES*, internal ribosome entry site; *pA*, polyadenylation signal. Co-infection with Adv-Cre removed the STOP cassette from Adv-LKB1. *B*, cellular levels of PAK1 autophosphorylation, total PAK1, and *in vitro* PAK1 activity in LKB1-expressing MEF3-2 cells. MEF 3-2 cells were co-infected with recombinant adenoviruses Adv-Cre and Adv-LKB1. Control cells were infected with Adv-Cre alone. The levels of phospho-PAK1 and PAK1 were determined by Western blotting with anti-phospho-PAK1 (Ser^{144})/PAK2 (Ser^{141}) and anti-PAK1 antibodies, respectively. Lysates were prepared from MEF3-2 cells infected with the indicated recombinant adenoviruses and immunoprecipitated using an anti-PAK1 antibody. The precipitates were used for *in vitro* kinase assays with GST-VASP-(158–277) as a substrate. The phosphorylation of GST-VASP was visualized and quantified using BAS-5000 Bio-imaging Analyzer. *Error bars* indicate S.D. The *asterisk* represents significant decreases compared with control cells ($p < 0.001$). *C*, the constitutively active mutant of PAK1 rescues LKB1-induced suppression of cell migration in MEF3-2 cells. MEF 3-2 cells were co-infected with recombinant adenoviruses Adv-Cre, Adv-LKB1, and Adv-PAK1-T423E at a multiplicity of infection of 5, 10, or 20. Control cells were infected with Adv-Cre alone. Cell migration assays were performed as Fig. 1. *Error bars* indicate S.D. The *asterisk* represents significant changes in Adv-Cre/Adv-LKB1/Adv-PAK1-T423E (5) infected cells compared with Adv-Cre/Adv-LKB1-infected cells ($p < 0.001$). Similar results were obtained in three independent experiments.

LKB1 suppressed metastasis of cancer cells, we determined the effect of LKB1 knockdown on cell migration using a wound-healing assay. As test cells, we used a human colon cancer cell line HCT116 that expressed a significant level of LKB1 endogenously. HCT116 cells transfected with LKB1 siRNA (1 and 2) migrated 1.5× faster than those with scrambled siRNA pool (Fig. 1, *A* and *B*, *Scr.*). Because PAK1 is an important regulator of cell migration (34), we investigated a possible role of PAK1 in cell migration enhanced by LKB1 knockdown. To determine the PAK1 activity in LKB1 knockdown cells, we then analyzed the level of phospho-PAK1 (Ser^{144}), its active form (35). Knockdown of LKB1 increased the cellular level of the phosphorylated PAK1, without affecting that of total PAK1 (Fig. 1*C*). These results suggest that knockdown of LKB1 increases the PAK1 activity. To confirm this interpretation, we determined the effect of LKB1 knockdown on *in vitro* PAK1 activity. Because histone H4, a widely used substrate for PAK1, was phosphorylated by LKB1 (data not shown), we screened *in silico* candidate substrate sequences for PAK1 using the consensus phosphorylation motif ((K/R)(R/*X*)(*X*)(pS/pT)) (34) as a query. As a candidate, we identified VASP-(158–277), which is a major substrate for both PKA and PKG (32, 36). We first verified that recombinant PAK1 efficiently phosphorylated GST-VASP-(158–277) (data not shown). We found that PAK1 activity was significantly higher in LKB1 knockdown cells than in the control cells (Fig. 1*C*). To further investigate whether enhanced PAK1 activity contributed to the cell migration increase in LKB1 knockdown cells, we tested the effect of a dominant-negative mutant PAK1-K299R in LKB1 knockdown cells. Notably, expression of PAK1-K299R suppressed the increase in migration of these cells (Fig. 1*D*). These results suggest that LKB1 inhibits PAK1 activity, which can suppress cell migration.

Expression of LKB1 in Lkb1-null MEFs Inhibits PAK1 Activity and Cell Migration—To investigate the role of LKB1 in suppression of PAK1-mediated signaling, we further evaluated the effect of forced LKB1 expression on PAK1 activation in mouse embryonic fibroblasts that lack wild-type LKB1 (MEF3-2). To this end, we used the recombinant adenovirus encoding LKB1/STRAD (Adv-LKB1) that contained a transcription termination cassette (STOP sequence) flanked by the *loxP* sequences and expressed LKB1/STRAD by co-infection of MEF3-2 with Adv-Cre, which removed the STOP sequence from Adv-LKB1. The floxed inducible system was employed because LKB1 had some cytotoxic effects on host HEK293 cells and hampered production of the LKB1-expressing recombinant adenovirus. Such cytotoxicity was not observed with MEF3-2 cells up to 48 h post-induction. (Fig. 2*A*) (17). The cells infected with Adv-LKB1 alone showed

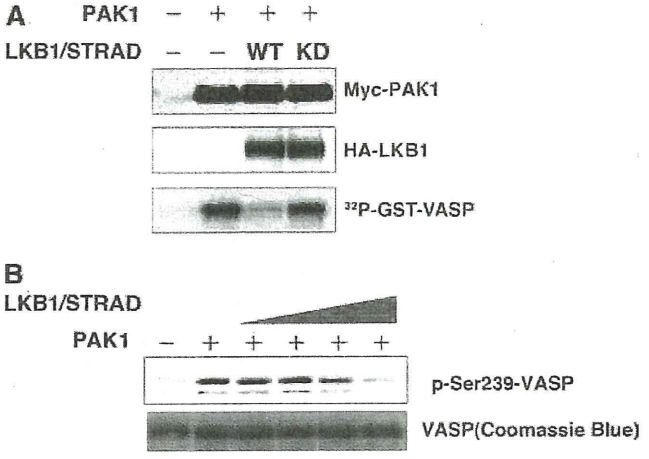

FIGURE 3. **LKB1 activity is necessary for suppression of PAK1 activity.** *A*, the wt LKB1, but not the kinase-dead mutant (*KD*), inhibits PAK1 activity. HEK293T cells were co-transfected with the indicated constructs. At 24 h post-transfection, immunoprecipitates were prepared with an anti-Myc antibody. The precipitates were used for *in vitro* kinase assays using GST-VASP-(158–277) as a substrate. The kinase activities were visualized using BAS-5000 Bio-imaging Analyzer. Cellular levels of Myc-PAK1 and HA-LKB1 were determined by Western blotting with anti-Myc or anti-HA antibody. *B*, recombinant LKB1 complex (LKB1-STRAD-MO25) directly inhibits PAK1 activity *in vitro* in a dose-dependent manner. The LKB1 complex (LKB1-STRAD-MO25) was preincubated with recombinant PAK1 and ATP in the absence of any PAK1 substrates, followed by addition of GST-VASP. The phosphorylated VASP was detected using an anti-phospho-VASP (Ser^{239}) antibody. Coomassie Brilliant Blue was used for detection of GST-VASP-(158–277). Similar results were obtained in three independent experiments.

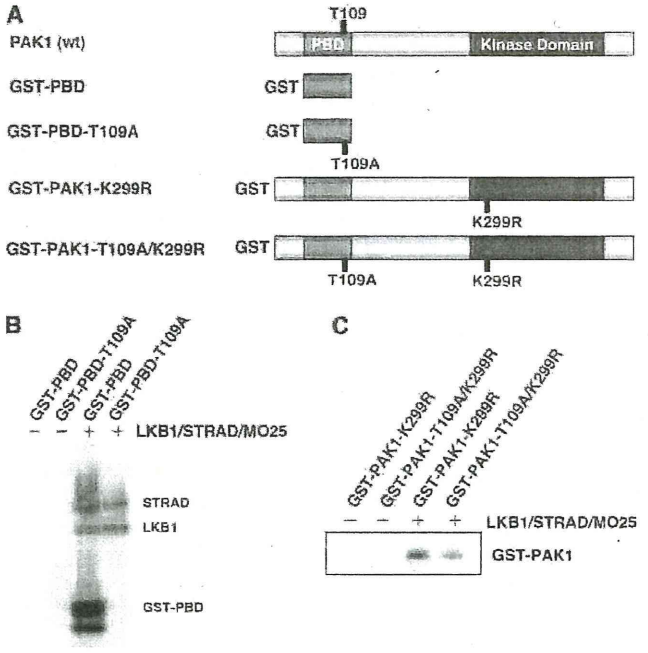

FIGURE 4. **LKB1 phosphorylates PAK1 *in vitro* at Thr^{109}.** *A*, schematic presentation of PAK1 and its mutant forms. wt PAK1 contains the p21-binding domain (*light gray*) and the kinase domain (*dark gray*). The noncatalytic domains are in *white*. Thr^{109} is a possible phosphorylation site for LKB1. *B*, LKB1 phosphorylates GST-PAK1-PBD at Thr^{109} *in vitro*. The recombinant LKB1 complex (LKB1-STRAD-MO25) was incubated with GST-PBD or GST-PBD-T109A. *C*, LKB1 phosphorylates full-length GST-PAK1-K299R and GST-PAK1-T109A/K299R to a lesser extent. The *in vitro* kinase assays were performed using the recombinant LKB1 complex with GST-PAK1-K299R or GST-PAK1-T109A/K299R. The phosphorylation of the indicated recombinant proteins was visualized using BAS-5000 Bio-imaging Analyzer. These experiments were repeated at least twice with similar results.

similar activity of PAK1 to those infected with Adv-Cre alone (control cells) (Fig. 2*B*). Notably, forced expression of LKB1/STRAD by co-infection of Adv-LKB1 and Adv-Cre decreased the cellular level of the phosphorylated PAK1 but not that of total PAK1 and inhibited the PAK1 activity by ~60% as compared with that in the control cells infected with Adv-Cre or Adv-LKB1 alone (Fig. 2*B*). Furthermore, forced expression of LKB1/STRAD reduced cell migration in MEF3-2 cells (to 35% of Adv-Cre alone) (Fig. 2*C*). To directly test whether LKB1 reduces cell migration through inhibition of PAK1, we infected MEF3-2 cells with various multiplicity of infection of the adenovirus encoding the constitutively active mutant of PAK1 (Adv-PAK1-T423E) together with Adv-Cre/Adv-LKB1. Co-infection with Adv-PAK1-T423E has recovered the LKB1-induced reduction of cell migration in a dose-dependent manner (Fig. 2*C*). These results suggest that LKB1 can contribute to the suppression of cell migration through inhibition of PAK1.

LKB1 Activity Is Necessary for Suppression of PAK1—PAK1 can be activated by recruitment of the active forms of Cdc42/Rac and phosphorylation by 3-phosphoinositide-dependent kinase-1 (19). Thus, we investigated whether the protein kinase activity of LKB1 was necessary to suppress the PAK1 activation. HEK293T cells were transiently transfected with PAK1 and/or LKB1/STRAD expression vector to determine PAK1 activity. The wild-type LKB1 (wt) inhibited the activity significantly, whereas the kinase-dead mutant of LKB1 (kinase-dead) did not affect activity (Fig. 3*A*). These results indicated that LKB1 activity was necessary for PAK1 inhibition. Accordingly, we next hypothesized that LKB1-mediated phosphorylation of PAK1 reduced its kinase activity. To test the possibility, we preincubated recombinant PAK1 with various amounts of LKB1 in the presence of ATP and then added the substrate of PAK1 to determine its kinase activity. LKB1 directly inhibited the PAK1 activity *in vitro* in a dose-dependent manner (Fig. 3*B*). These results indicate that LKB1-mediated PAK1 phosphorylation decreases its kinase activity.

LKB1 Can Phosphorylate PAK1 at Thr^{109}—To study PAK1 phosphorylation by LKB1 further, we searched the LKB1 substrate amino acid sequence motif "L*X*T" (5, 37) in full-length PAK1. We found an LQT sequence (107–109) within the p21-binding domain (PBD) in the regulatory region located near the N terminus of PAK1 (Fig. 4*A*). To determine whether Thr^{109} of PAK1 could be phosphorylated by LKB1, we constructed a GST-fused PBD recombinant protein (GST-PBD) and its mutated form in PBD, GST-PBD-T109A (Fig. 4*A*). Recombinant LKB1 failed to phosphorylate GST-PBD-T109A *in vitro*, although it phosphorylated GST-PBD efficiently (Fig. 4*B*). Next, we tested whether LKB1 phosphorylated the full-length PAK1 at Thr^{109}. To this end, we used a full-length dominant-negative PAK1 recombinant protein (GST-PAK1-K299R) as the substrate to minimize the effect of autophosphorylation and introduced alanine substitution at Thr^{109}, GST-PAK1-K299R/T109A (Fig. 4*A*). The full-length PAK1 (GST-PAK1-K299R) was phosphorylated by LKB1 efficiently, whereas the GST-PAK1-K299R/T109A was at a much reduced level (Fig. 4*C*). These results suggest that full-length PAK1 can be a sub-

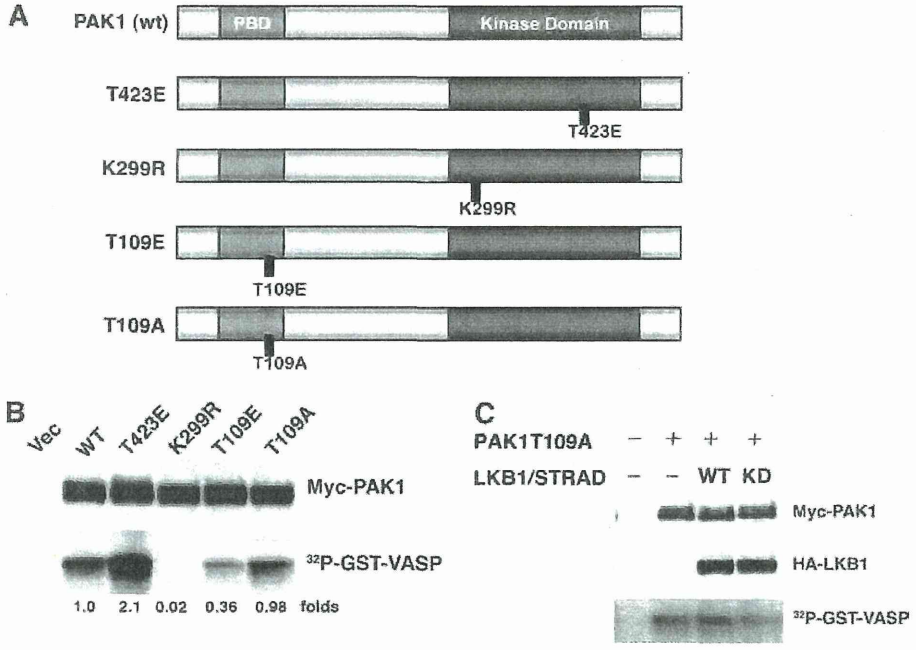

FIGURE 5. **Phosphorylation of PAK1 at Thr^{109} reduces its activity.** *A*, structures of PAK1 constructs. wt PAK1 contains the p21-binding domain (*light gray*) and the kinase domain (*dark gray*). The noncatalytic domains are in *white*. Also displayed are the constitutively active mutant (T423E), dominant-negative mutant (K299R), phosphorylation-mimicked mutant for Thr^{109} (T109E), and the nonphosphorylatable mutant for Thr^{109} (T109A). *B*, the kinase activities of PAK1 mutants. The HEK293T cells were co-transfected with the indicated constructs. At 24 h post-transfection, the immunoprecipitates were prepared with an anti-Myc antibody. The precipitates were used for *in vitro* kinase assays using GST-VASP-(158–277) as a substrate. Cellular levels of Myc-PAK1 were determined by Western blotting with anti-Myc antibody. *C*, LKB1 (wt or kinase-dead (*KD*)) failed to inhibit the activity of the PAK1-T109A mutant. Cultured HEK293T cells were co-transfected with the indicated constructs. The kinase activities were determined as described under "Experimental Procedures." Cellular levels of Myc-PAK1 and HA-LKB1 were determined by Western blotting with anti-Myc or anti-HA antibody. Similar results were obtained in three independent experiments. *Vec*, vector.

strate for LKB1 and that Thr^{109} is a likely target of phosphorylation by LKB1, although it is possible that LKB1 phosphorylates other residues of PAK1 in addition to Thr^{109}. To determine whether LKB1 phosphorylates PAK1 at Thr^{109} *in vivo*, we performed a series of mass spectrometric analyses of PAK1 purified from HEK293T cells transiently co-transfected with plasmids encoding PAK1 and LKB1/STRAD (supplemental Fig. S1). The protonated molecular ions of peptide LLQTSNITK-(106–114) obtained from tryptic digestion of wt-PAK1 were detected in its nonphosphorylated form ($[M + H]^+$ at *m/z* 1017.55) and in its monophosphorylated form ($[M + H]^+$ at *m/z* 1097.54). To further confirm the specific phosphorylation site of the peptide, we used HEK293T cells co-transfected with plasmids encoding PAK1-T109A and LKB1/STRAD for another set of mass spectrometric analyses. The molecular ion of LLQASNITK appeared at *m/z* 987.59 corresponding to the substitution of threonine at residue 109 with alanine. Notably, the corresponding monophosphopeptide was not detected in PAK1-T109A, excluding phosphorylation at the other Thr or Ser residue of the peptide. These results are consistent with our interpretation that LKB1 phosphorylates PAK1 at Thr^{109} *in vivo*.

Phosphorylation of PAK1 at Thr^{109} by LKB1 Reduces Its Activity—We have demonstrated that the kinase activity of LKB1 is necessary to inhibit that of PAK1 (Fig. 3*A*). Therefore, we next investigated whether phosphorylation of Thr^{109} by LKB1 regulated PAK1 activity. Namely, we constructed a PAK1-T109E mutant whose amino acid residue 109 was converted to glutamic acid from threonine. This substitution mimics the phosphorylation of threonine with the acidic moiety of glutamic acid. As an inactive (negative) control, we also constructed the alanine substitution PAK1-T109A (Fig. 5*A*). We transiently transfected HEK293T cells with plasmids encoding these constructs of PAK1: wt, constitutively-active (T423E), dominant-negative (K299R), T109E, and T109A, respectively (Fig. 5*A*). We then determined the *in vitro* PAK1 activities in the cell lysates using GST-VASP-(158–277) as substrate. The PAK1 mutant T423E showed the highest activity (2.1×), whereas mutant K299R with defective kinase (kinase-dead) had only 2% of the wt-PAK1 activity. Notably, T109E mutant showed significantly reduced PAK1 activity (36% of wt), whereas T109A mutant had a similar activity to the wt (98%) (Fig. 5*B*). These results suggest that phosphorylation of PAK1 at Thr^{109} decreases its kinase activity. To confirm the role of phosphorylation at Thr^{109} in suppression of PAK1 activity by LKB1, we next tested nonphosphorylatable PAK1-T109A in HEK293T cells. Co-expression of LKB1 failed to suppress the activity of PAK1-T109A (Fig. 5*C*), in sharp contrast to the effect on wt-PAK1 (Fig. 3*A*). These results strongly suggest that LKB1 suppresses the PAK1 activity by phosphorylating it at Thr^{109}.

Activation of PAK1 in Lkb1(+/−) Mouse HCCs and Lkb1(−/−) MEFs—We have previously demonstrated that *Lkb1*(+/−) mice develop HCC after 50 weeks of age and that HCCs and nodular foci of *Lkb1*(+/−) liver show loss of the *Lkb1* heterozygosity (10, 11). To test the involvement of LKB1 in PAK1-mediated signaling *in vivo*, we next determined the level of phosphorylated form of PAK1 in HCCs of *Lkb1*(+/−) mice, using two different types of phospho-specific PAK1 antibodies that recognized the active form of PAK1. Notably, we found that the level of phosphorylated PAK1 was increased in HCCs (H1 and H2) and in precancerous lesions (nodular foci, F1 and F2), compared with the normal liver of *Lkb1*(+/−) or *Lkb1*(+/+) mice, while the levels of total PAK1 in nodular foci and HCCs were similar to those in normal liver (Fig. 6*A*). These results are therefore consistent with the interpretation that loss of LKB1 induces PAK1 activation. We further investigated the status of PAK1 activation in *Lkb1*(−/−) MEFs (MEF3-2) and wt MEFs. Both the level of phosphorylated PAK1 and *in vitro* PAK1 activity were significantly higher in *Lkb1*(−/−) MEFs

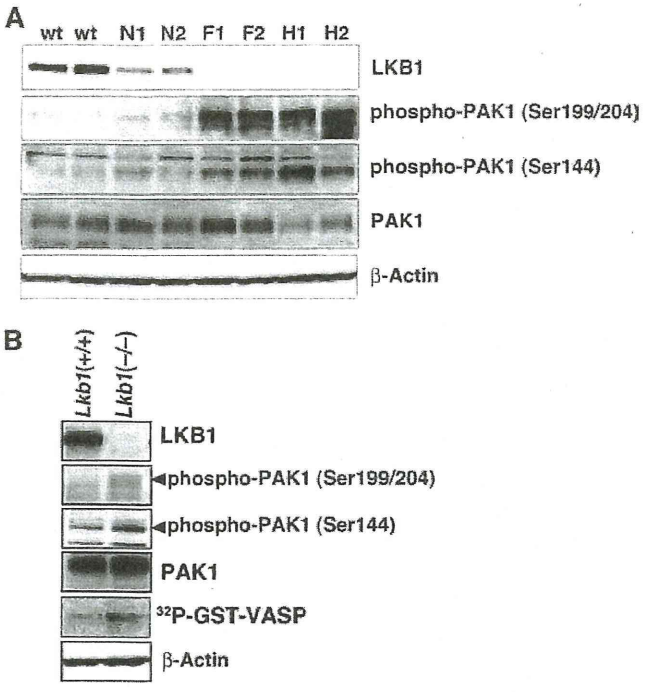

FIGURE 6. **Activation of PAK1 in *Lkb1*(+/−) mouse HCCs and *Lkb1*(−/−) MEFs.** *A*, activation of PAK1 in *Lkb1*(+/−) mice HCCs. Cellular levels of phospho-PAK1, PAK1, and β-actin in tissue lysates were determined by Western blotting with anti-phospho-PAK1 (Ser^{144}), anti-phospho-PAK1 ($Ser^{199/204}$), anti-PAK1, and anti-β-actin. Two wild-type livers (W1 and W2), pairs of tumor (H1 and H2), precancerous lesions (F1 and F2) and adjacent normal tissue (N1 and N2) from two *Lkb1*(+/−) mice were analyzed. *B*, increased PAK1 activity in *Lkb1*(−/−) MEFs. Cellular levels of phospho-PAK1, PAK1, and β-actin in tissue lysates were determined by Western blotting with the indicated antibodies. For *in vitro* kinase assay, cell lysates were prepared from MEF cells and immunoprecipitated using an anti-PAK1 antibody. The precipitates were used for *in vitro* kinase assays using GST-VASP-(158–277) as a substrate. The phosphorylation of GST-VASP was visualized using BAS-5000 Bio-imaging Analyzer. Similar results were obtained in three independent experiments.

than those in wt MEFs (Fig. 6*B*). These data together suggest that loss of LKB1 contributes to the activation of PAK1.

DISCUSSION

In this study, we have provided evidence that LKB1 inhibits PAK1 activation by direct phosphorylation of PAK1 at Thr^{109}. We first showed that knockdown of LKB1 increased cell migration and PAK1 activity in HCT116 cells (Fig. 1), whereas introduction of LKB1 in *Lkb1*-null MEFs reduced cell migration and PAK1 activity simultaneously (Fig. 2). Notably, a constitutively active mutant of PAK1 (PAK1-T423E) recovered the LKB1-mediated reduction of cell migration in a dose-dependent manner (Fig. 2*C*). Because HCCs in *Lkb1*(+/−) mice can metastasize to the lung (10), it is conceivable that inhibition of PAK1 by LKB1 contributes to suppression of cancer metastasis. We also demonstrated that LKB1 directly phosphorylated PAK1 at Thr^{109} both *in vitro* (Fig. 4) and *in vivo* (supplemental Fig. S1). Importantly, the phosphomimetic PAK1-T109E mutation reduced its activity (Fig. 5*B*), whereas the activity of a nonphosphorylatable mutant PAK1-T109A was not suppressed by LKB1 (Fig. 5*C*). These results indicate that phosphorylation of Thr^{109} is both necessary and sufficient for inhibition of PAK1 activity by LKB1, although it is possible that LKB1 phosphorylates other residues of PAK1 in addition to Thr^{109} (Fig. 4*C*). Consistently, we found that active forms of PAK1 were increased in the nodular foci and HCCs in *Lkb1*(+/−) mice, compared with the normal liver of *Lkb1*(+/−) and *Lkb1*(+/+) mice (Fig. 6*A*).

Our present results indicate that PAK1 is a novel LKB1 substrate. So far, 14 kinases have been identified as LKB1 substrates, including AMPKα1, AMPKα2, MARK1, and MARK2. LKB1 phosphorylates these kinases at the L*X*T motif in the activation loop (5, 37), and such phosphorylations can induce kinase activation. In contrast, LKB1-induced phosphorylation of PAK1 at Thr^{109} in the L*X*T motif of PBD causes a decrease in the kinase activity (Fig. 5*B*). Because this motif is well conserved among group I PAKs (PAK1, PAK2, and PAK3), it is likely that regulation of the PAK1 activity by LKB1 applies to PAK2 and PAK3 as well. According to the structural analysis of PAK1, Thr^{109} is located at the helix loop Iα in an inhibitory switch (38) and exposed to the outer space. In addition, the L107F mutation of PAK1 prevents the interaction between the autoinhibitory region and the C-terminal catalytic region, making the constitutively active kinase (39). Because this mutant lacks the L*X*T motif, the constitutive activation is likely due to the loss of negative regulation by LKB1. We therefore speculate that the phosphorylation of this Thr residue enhances the interaction between the autoinhibitory (N-terminal regulatory) and kinase domains, leading to inhibition of the PAK1 activity. Further experiments are required to elucidate the precise role of Thr^{109} phosphorylation in PAK1 conformation.

It has been reported recently that LKB1 maintains cancer cell polarity by recruiting Cdc42 to the leading edges and that inhibition of LKB1 reduces PAK1 autophosphorylation (40). In contrast, we have found that LKB1 suppresses PAK1 activity by direct phosphorylation. The reason for the discrepancy is not clear but may be related to the methods used to overexpress LKB1 (transient transfection of LKB1 expression vector alone *versus* co-infection of LKB1 with STRAD using adenovirus vector) or the cell context, genetic constitution such as p53 mutation status (non-small cell lung cancer cells (p53 mutant) *versus* HEK293T or *Lkb1*-null MEFs (wt-p53)). Notably, LKB1 plays key roles in growth arrest or apoptosis through a p53-dependent mechanism (41, 42). Thus, it is conceivable that LKB1-mediated PAK1 inhibition may be dependent on the p53 status.

Numerous PAK1 substrates and/or interacting proteins have been identified that activate diverse signaling processes involved in cell motility, morphology, growth, survival, and epithelial-mesenchymal transition (19). For example, PAK1 stabilizes microtubules through stathmin/Op18 phosphorylation (43, 44). Therefore, LKB1 also may contribute to microtubule destabilization by regulating PAK1, whereas we have reported previously that LKB1 inhibits tubulin polymerization through activation of MARK2 (17). Further investigation is needed to address the role of LKB1 in various downstream processes of PAK1 other than cell motility. In conclusion, our present results suggest that PAK1 is a novel downstream target of LKB1, and that LKB1-mediated PAK1 phosphorylation may play important roles in tumor suppression in the liver.

Acknowledgment—We thank Dr. J. Chernoff for PAK1 wild-type, T423E, H83LH86LK299R, and 86L-K299R constructs.

REFERENCES

1. Giardiello, F. M., Welsh, S. B., Hamilton, S. R., Offerhaus, G. J., Gittelsohn, A. M., Booker, S. V., Krush, A. J., Yardley, J. H., and Luk, G. D. (1987) *N. Engl. J. Med.* **316,** 1511–1514
2. Hemminki, A., Markie, D., Tomlinson, I., Avizienyte, E., Roth, S., Loukola, A., Bignell, G., Warren, W., Aminoff, M., Höglund, P., Järvinen, H., Kristo, P., Pelin, K., Ridanpää, M., Salovaara, R., Toro, T., Bodmer, W., Olschwang, S., Olsen, A. S., Stratton, M. R., de la Chapelle, A., and Aaltonen, L. A. (1998) *Nature* **391,** 184–187
3. Jenne, D. E., Reimann, H., Nezu, J., Friedel, W., Loff, S., Jeschke, R., Müller, O., Back, W., and Zimmer, M. (1998) *Nat. Genet.* **18,** 38–43
4. Launonen, V. (2005) *Hum. Mutat.* **26,** 291–297
5. Alessi, D. R., Sakamoto, K., and Bayascas, J. R. (2006) *Annu. Rev. Biochem.* **75,** 137–163
6. Katajisto, P., Vallenius, T., Vaahtomeri, K., Ekman, N., Udd, L., Tiainen, M., and Mäkelä, T. P. (2007) *Biochim. Biophys. Acta* **1775,** 63–75
7. Miyoshi, H., Nakau, M., Ishikawa, T. O., Seldin, M. F., Oshima, M., and Taketo, M. M. (2002) *Cancer Res.* **62,** 2261–2266
8. Rossi, D. J., Ylikorkala, A., Korsisaari, N., Salovaara, R., Luukko, K., Launonen, V., Henkemeyer, M., Ristimaki, A., Aaltonen, L. A., and Makela, T. P. (2002) *Proc. Natl. Acad. Sci. U.S.A.* **99,** 12327–12332
9. Bardeesy, N., Sinha, M., Hezel, A. F., Signoretti, S., Hathaway, N. A., Sharpless, N. E., Loda, M., Carrasco, D. R., and DePinho, R. A. (2002) *Nature* **419,** 162–167
10. Nakau, M., Miyoshi, H., Seldin, M. F., Imamura, M., Oshima, M., and Taketo, M. M. (2002) *Cancer Res.* **62,** 4549–4553
11. Miyoshi, H., Deguchi, A., Nakau, M., Kojima, Y., Mori, A., Oshima, M., Aoki, M., and Taketo, M. M., (2009) *Cancer Sci.* **100,** 2046–2053
12. Baas, A. F., Boudeau, J., Sapkota, G. P., Smit, L., Medema, R., Morrice, N. A., Alessi, D. R., and Clevers, H. C. (2003) *EMBO J.* **22,** 3062–3072
13. Boudeau, J., Baas, A. F., Deak, M., Morrice, N. A., Kieloch, A., Schutkowski, M., Prescott, A. R., Clevers, H. C., and Alessi, D. R. (2003) *EMBO J.* **22,** 5102–5114
14. Baas, A. F., Smit, L., and Clevers, H. (2004) *Trends. Cell Biol.* **14,** 312–319
15. Zhang, L., Li, J., Young, L. H., and Caplan, M. J. (2006) *Proc. Natl. Acad. Sci. U.S.A.* **103,** 17272–17277
16. Zheng, B., and Cantley, L. C. (2007) *Proc. Natl. Acad. Sci. U.S.A.* **104,** 819–822
17. Kojima, Y., Miyoshi, H., Clevers, H. C., Oshima, M., Aoki, M., and Taketo, M. M. (2007) *J. Biol. Chem.* **282,** 23532–23540
18. Partin, A. W., Isaacs, J. T., Treiger, B., and Coffey, D. S. (1988) *Cancer Res.* **48,** 6050–6053
19. Bokoch, G. M. (2003) *Annu. Rev. Biochem.* **72,** 743–781
20. Kumar, R., Gururaj, A. E., and Barnes, C. J. (2006) *Nat. Rev. Cancer* **6,** 459–471
21. Manser, E., Leung, T., Salihuddin, H., Zhao, Z. S., and Lim, L. (1994) *Nature* **367,** 40–46
22. Tsakiridis, T., Taha, C., Grinstein, S., and Klip, A. (1996) *J. Biol. Chem.* **271,** 19664–19667
23. King, C. C., Gardiner, E. M., Zenke, F. T., Bohl, B. P., Newton, A. C., Hemmings, B. A., and Bokoch, G. M. (2000) *J. Biol. Chem.* **275,** 41201–41209
24. Tang, Y., Zhou, H., Chen, A., Pittman, R. N., and Field, J. (2000) *J. Biol. Chem.* **275,** 9106–9109
25. Balasenthil, S., Sahin, A. A., Barnes, C. J., Wang, R. A., Pestell, R. G., Vadlamudi, R. K., and Kumar, R. (2004) *J. Biol. Chem.* **279,** 1422–1428
26. Holm, C., Rayala, S., Jirström, K., Stål, O., Kumar, R., and Landberg, G. (2006) *J. Natl. Cancer Inst.* **98,** 671–680
27. Carter, J. H., Douglass, L. E., Deddens, J. A., Colligan, B. M., Bhatt, T. R., Pemberton, J. O., Konicek, S., Hom, J., Marshall, M., and Graff, J. R. (2004) *Clin. Cancer Res.* **10,** 3448–3456
28. Ching, Y. P., Leong, V. Y., Lee, M. F., Xu, H. T., Jin, D. Y., and Ng, I. O. (2007) *Cancer Res.* **67,** 3601–3608
29. Wang, R. A., Zhang, H., Balasenthil, S., Medina, D., and Kumar, R. (2006) *Oncogene* **25,** 2931–2936
30. Sapkota, G. P., Kieloch, A., Lizcano, J. M., Lain, S., Arthur, J. S., Williams, M. R., Morrice, N., Deak, M., and Alessi, D. R. (2001) *J. Biol. Chem.* **276,** 19469–19482
31. Sandig, V., Youil, R., Bett, A. J., Franlin, L. L., Oshima, M., Maione, D., Wang, F., Metzker, M. L., Savino, R., and Caskey, C. T. (2000) *Proc. Natl. Acad. Sci. U.S.A.* **97,** 1002–1007
32. Deguchi, A., Soh, J. W., Li, H., Pamukcu, R., Thompson, W. J., and Weinstein, I. B. (2002) *Mol. Cancer. Ther.* **1,** 803–809
33. Ji, H., Ramsey, M. R., Hayes, D. N., Fan, C., McNamara, K., Kozlowski, P., Torrice, C., Wu, M. C., Shimamura, T., Perera, S. A., Liang, M. C., Cai, D., Naumov, G. N., Bao, L., Contreras, C. M., Li, D., Chen, L., Krishnamurthy, J., Koivunen, J., Chirieac, L. R., Padera, R. F., Bronson, R. T., Lindeman, N. I., Christiani, D. C., Lin, X., Shapiro, G. I., Jänne, P. A., Johnson, B. E., Meyerson, M., Kwiatkowski, D. J., Castrillon, D. H., Bardeesy, N., Sharpless, N. E., and Wong, K. K. (2007) *Nature* **448,** 807–810
34. Kumar, R., and Vadlamudi, R. K. (2002) *J. Cell. Physiol.* **193,** 133–144
35. Chong, C., Tan, L., Lim, L., and Manser, E. (2001) *J. Biol. Chem.* **276,** 17347–17353
36. Butt, E., Abel, K., Krieger, M., Palm, D., Hoppe, V., Hoppe, J., and Walter, U. (1994) *J. Biol. Chem.* **269,** 14509–14517
37. Lizcano, J. M., Göransson, O., Toth, R., Deak, M., Morrice, N. A., Boudeau, J., Hawley, S. A., Udd, L., Mäkelä, T. P., Hardie, D. G., and Alessi, D. R. (2004) *EMBO J.* **23,** 833–843
38. Lei, M., Lu, W., Meng, W., Parrini, M. C., Eck, M. J., Mayer, B. J., and Harrison, S. C. (2000) *Cell* **102,** 387–397
39. Brown, J. L., Stowers, L., Baer, M., Trejo, J., Coughlin, S., and Chant, J. (1996) *Curr. Biol.* **6,** 598–605
40. Zhang, S., Schafer-Hales, K., Khuri, F. R., Zhou, W., Vertino, P. M., and Marcus, A. I. (2008) *Cancer Res.* **68,** 740–748
41. Karuman, P., Gozani, O., Odze, R. D., Zhou, X. C., Zhu, H., Shaw, R., Brien, T. P., Bozzuto, C. D., Ooi, D., Cantley, L. C., and Yuan, J. (2001) *Mol. Cell* **7,** 1307–1319
42. Tiainen, M., Ylikorkala, A., and Mäkelä, T. P. (1999) *Proc. Natl. Acad. Sci. U.S.A.* **96,** 9248–9251
43. Belmont, L. D., and Mitchison, T. J. (1996) *Cell* **84,** 623–631
44. Larsson, N., Marklund, U., Gradin, H. M., Brattsand, G., and Gullberg, M. (1997) *Mol. Cell. Biol.* **17,** 5530–5539

OPEN ACCESS Freely available online PLoS GENETICS

A Mutation in the Gene Encoding Mitochondrial Mg^{2+} Channel MRS2 Results in Demyelination in the Rat

Takashi Kuramoto[1]*, Mitsuru Kuwamura[2], Satoko Tokuda[1,2], Takeshi Izawa[2], Yoshifumi Nakane[1], Kazuhiro Kitada[1,3], Masaharu Akao[4], Jean-Louis Guénet[5], Tadao Serikawa[1]

1 Institute of Laboratory Animals, Graduate School of Medicine, Kyoto University, Kyoto, Japan, **2** Laboratory of Veterinary Pathology, Osaka Prefecture University, Osaka, Japan, **3** Laboratory of Mammalian Genetics, Genome Dynamics Research Center, Graduate School of Science, Hokkaido University, Sapporo, Japan, **4** Department of Cardiovascular Medicine, Graduate School of Medicine, Kyoto University, Kyoto, Japan, **5** Département de Biologie du Développement, Institut Pasteur, Paris, France

Abstract

The rat demyelination (*dmy*) mutation serves as a unique model system to investigate the maintenance of myelin, because it provokes severe myelin breakdown in the central nervous system (CNS) after normal postnatal completion of myelination. Here, we report the molecular characterization of this mutation and discuss the possible pathomechanisms underlying demyelination. By positional cloning, we found that a G-to-A transition, 177 bp downstream of exon 3 of the *Mrs2* (MRS2 magnesium homeostasis factor (*Saccharomyces cerevisiae*)) gene, generated a novel splice acceptor site which resulted in functional inactivation of the mutant allele. Transgenic rescue with wild-type *Mrs2*-cDNA validated our findings. *Mrs2* encodes an essential component of the major Mg^{2+} influx system in mitochondria of yeast as well as human cells. We showed that the *dmy/dmy* rats have major mitochondrial deficits with a markedly elevated lactic acid concentration in the cerebrospinal fluid, a 60% reduction in ATP, and increased numbers of mitochondria in the swollen cytoplasm of oligodendrocytes. MRS2-GFP recombinant BAC transgenic rats showed that MRS2 was dominantly expressed in neurons rather than oligodendrocytes and was ultrastructurally observed in the inner membrane of mitochondria. Our observations led to the conclusion that *dmy/dmy* rats suffer from a mitochondrial disease and that the maintenance of myelin has a different mechanism from its initial production. They also established that Mg^{2+} homeostasis in CNS mitochondria is essential for the maintenance of myelin.

Citation: Kuramoto T, Kuwamura M, Tokuda S, Izawa T, Nakane Y, et al. (2011) A Mutation in the Gene Encoding Mitochondrial Mg^{2+} Channel MRS2 Results in Demyelination in the Rat. PLoS Genet 7(1): e1001262. doi:10.1371/journal.pgen.1001262

Editor: Gregory S. Barsh, Stanford University, United States of America

Received June 5, 2010; **Accepted** November 29, 2010; **Published** January 6, 2011

Funding: This work was supported by grants-in-aid for Scientific Research from the Japan Society for the Promotion of Science [21300153 to TK] and a grant-in-aid for Cancer Research from the Ministry of Health, Labour, and Welfare. The funders had no role in study design, data collection and analysis, decision to publish, or preparation of the manuscript.

Competing Interests: The authors have declared that no competing interests exist.

* E-mail: tkuramot@anim.med.kyoto-u.ac.jp

Introduction

Myelin is an essential component of the nervous tissue of higher vertebrates. It acts as a natural insulator of axonal segments allowing, at the same time, the maintenance of axonal integrity and the fast conduction of action potentials. It also reduces ionic currents across the axonal membrane and stabilizes the extracellular milieu within rapidly-firing axon bundles.

In the central nervous system (CNS), myelin is produced by oligodendrocytes, while in the peripheral nervous system (PNS), this function is achieved by Schwann cells. Myelination is completed within a relatively short period of time during mammalian development and requires a high rate of production and transport of different kinds of molecules, mostly proteins and lipids. In adult life, myelin is constantly remodeled and the maintenance of functional myelin sheaths requires a careful balance of *de novo* synthesis and turnover. It is quite clear that any event generating an imbalance in the myelination or remyelination process has the greatest chance of inducing dys- or demyelination of either the central or peripheral nervous system.

Our knowledge of the myelination process has benefited from careful observations conducted on human patients affected by one of the many defects of myelination or myelin turnover. It has also benefited from researches carried out on animal models, mostly mutant mice and rats, including those that have been induced by transgenesis or genetic engineering in ES cell lines [1,2]. Some of these models have even allowed therapies to be developed in a preclinical setting [3]. Unfortunately, only a small number of the many genes that are directly or indirectly involved in the myelination process have been identified and only a few of these genes have been functionally annotated, for example, by the characterization of one or more mutant alleles. For this reason, any new mutation occurring spontaneously or after mutagenesis is of potential interest for unraveling the molecular mechanisms involved in myelin assembly.

In an earlier paper we reported the discovery and pathology of a rat mutation designated *demyelination* (symbol *dmy*), which is characterized by severe and progressive myelin breakdown in the CNS. We mapped the locus responsible for this myelin disorder to rat chromosome (Chr) 17, very close to the prolactin (*Prl*) locus, in a region homologous to human Chr 6p21.1-22.3 and mouse Chr 13 [4,5]. Based on its pathological features, as well as its genetic localization, this demyelination syndrome appeared to be unique, with no homologue so far reported in any other mammalian species, including humans.

Author Summary

The myelin sheath that surrounds the axon of a neuron acts as a biological insulator. Its major function is to increase the speed at which impulses propagate along myelinated fibers in the central nervous system, as well as the peripheral nervous system. Alterations or damage affecting this structure (demyelination) result in the disruption of signals between the brain and other parts of the body. In the rat, mutations producing demyelination have been frequently identified and characterized and have contributed to a better understanding of the genetics of myelin development, physiology, and pathology. This paper reports the molecular characterization of a recessive allele responsible for the progressive disruption of myelin that was initially observed in mutant rats, previously named demyelination (*dmy*). This mutation generates an additional splicing acceptor site in an intron of the mitochondrial Mg^{2+} transporter gene (*Mrs2*), resulting in the insertion of a 83-bp genomic DNA segment into the *Mrs2* transcript and complete functional inactivation of the mutant allele. We firstly defined the biological function of MRS2 in mammals and demonstrated the crucial and unexpected role of MRS2 in myelin physiology. Our findings might be helpful in the development of new therapeutic strategies for demyelinating syndromes.

In this report we demonstrate that the causative gene (*Mrs2*) encodes a protein that is an essential component of the major electrophoretic Mg^{2+} influx system in mitochondria [6]. This gene has orthologues in other organisms, including lower eukaryotes and plants [7,8]. The protein shares many of the properties of bacterial CorA and yeast Alr1 proteins but its specific involvement in the myelination process was not known or even suspected.

Results

dmy/dmy rats exhibit a phenotype with typical demyelination

The pathology of homozygous *dmy/dmy* rats has been reported in detail previously [4]. Mutant rats exhibit no significant differences from their control littermates until 4 weeks of age. From 5 weeks on, flaccidity of the hind limbs becomes noticeable and evolves towards complete paralysis around 7–8 weeks of age. Progressive demyelination is observed in several parts of the CNS (Figure 1), namely the corpus callosum, the capsula interna, the striatum and the cerebellar peduncle, with major effects on the ventral and lateral parts of the spinal cord. Astrogliosis, which is a major feature of myelin disorder, is observed in demyelinated areas but motor neurons remain normal and there is no sign of associated inflammation in the white matter. The *dmy* mutation can then be regarded as a mutation affecting the maintenance and turnover of myelin rather than its initial production: this is typical demyelination [9].

The *dmy* syndrome is associated with a mutation in a splicing site of *Mrs2*, a gene encoding a mitochondrial Mg^{2+} channel

Out of 687 *dmy/dmy* mutant rats, collected from the 3,252 offspring of an intercross segregating for the *dmy* mutation, 23 individuals were found to carry a recombinant haplotype between the two loci that were used for the initial genetic mapping, namely; *Prl* (prolactin) and *Hh1tts* (testis-specific histone, H1t). Further investigation of these animals, using three novel informative SSLP markers, allowed us to narrow the genetic interval containing *dmy* down to 0.22 cM, between markers *D17Kur17* and *D17Got45*. Within this critical section, we found no recombination between the *dmy* locus and either *Aldh5a1* (aldhehyde dehydrogenase family 5, subfamily A1) or *Mrs2* (mitochondrial 118 RNA splicing2) loci, among $687 \times 2 = 1{,}374$ meioses. The rat genome databases revealed that *D17Kur17* and *D17Got45* were at position 46.78-Mb and 47.26-Mb, respectively, on rat Chr 17, yielding a physical size of 0.48 Mb of DNA for the interval containing the *dmy* locus. This stretch of DNA contained 6 genes (Figure 2A).

Analysis by RT-PCR of the transcription products of these 6 genes revealed that the cDNA transcribed from the *Mrs2* gene was larger in *dmy/dmy* mutants than in the controls (Figure 2B). After sequencing, we found that the larger size of the *dmy* cDNA was due to the insertion of an 83 bp intronic sequence between exons 3 and 4. Comparison of the two genomic sequences revealed a G-to-A transition, 177 bp downstream of the end of exon 3 (Figure 2C, Figure S1), generating a novel splice acceptor site, which accounted for the addition of the 83bp stretch of intronic sequence to the mutant transcript. In addition, while the *Mrs2* gene normally encodes a 434 amino-acid protein, the intronic insertion leads to a shorter protein (106 amino acids) due to the occurrence of a stop codon as a consequence of frame shifting within the novel pseudo-exon X. The new protein consisted of the first 91 amino acids of normal (wild-type) MRS2 protein followed by an additional 15 amino acids transcribed from the intronic stretch (Figure 2D) [10]. No nucleotide alteration was observed between normal and mutant haplotypes in the cDNA transcribed from the other 5 genes (*Vmp*, *Dcdc2*, *Gpld1*, *Aldh5a1*, and *KIAA0319*). These findings strongly suggested that the G-to-A mutation in intron 3 of *Mrs2* in *dmy/dmy* rats was very likely causative of the neurological phenotype.

dmy/dmy rats exhibit morphological and biochemical features characteristic of mitochondrial deficiencies

The MRS2 protein functions as a major transporter protein (Mg^{2+}, Ni^{2+} and Co^{2+}) in yeast as well as in human cells [10,11]. When this protein is functionally defective this leads to the "petite" phenotype in yeast and to cell death in human HEK 293 cells [11,12]. Because mitochondrial diseases in mammals are often accompanied by elevated lactic acid, reduced ATP, increased cytochrome oxidase (COX) activity, and the morphological alteration of mitochondria [13–15], we measured lactic acid levels and ATP contents in the CNS and performed morphological analyses of the CNS of *dmy/dmy* rats.

Lactic acid concentration in the cerebrospinal fluids was significantly elevated in *dmy/dmy* rats when compared with normal littermates: 126 ± 43.7 mg/dL vs 25 ± 9.6 mg/dL (average $\pm$ SD), $P<0.002$ (Figure 3A). The ATP concentration was markedly reduced in *dmy/dmy* rats: 265 ± 79 μM/mg vs 99 ± 46 μM/mg (average $\pm$ SD), $P<0.005$ (Figure 3B). In the affected *dmy/dmy* rats, swollen oligodendrocytes were often observed in the white matter, showing the increased COX reaction products (Figure 3C). Ultrastructurally, their cytoplasm contained many mitochondria and Golgi apparatus-like membrane structures (Figure 3D). These findings indicated that the mitochondria of *dmy/dmy* rats were functionally defective.

Rescue of *dmy/dmy* mutant phenotypes by transgenic complementation

To ascertain that the molecular defect (*i.e.* G-to-A transition) observed in the *dmy* mutant haplotype was causative of the abnormal phenotype observed in *dmy/dmy* rats, we attempted to rescue the mutant phenotype by transgenic complementation. We

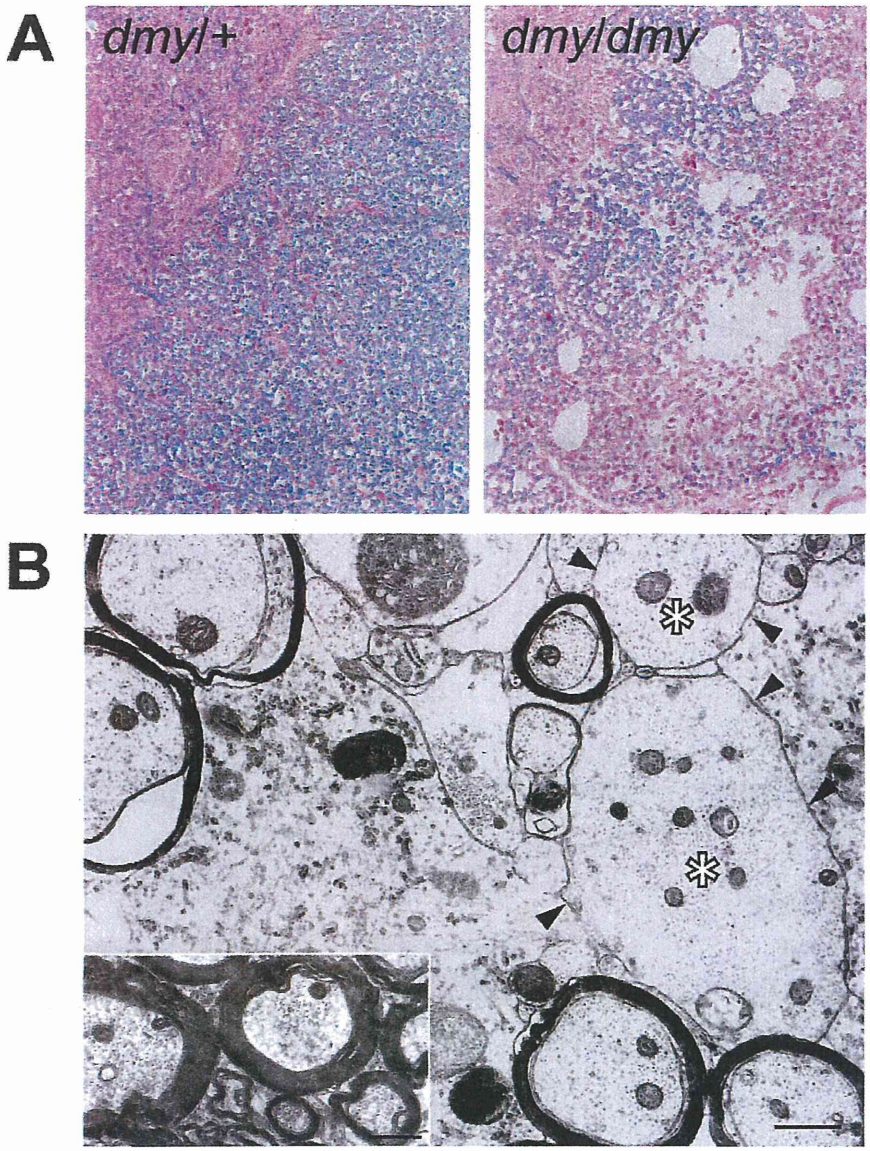

Figure 1. Demyelination in *dmy/dmy* rats. A. Histopathology of the cervical part of the spinal cord of *dmy/+* (left) and *dmy/dmy* (right) rats aged 10 weeks. Luxol fast blue-HE staining. Original magnification: ×100. B. Electron microscopy of the cervical part of spinal cord of *dmy/dmy* rats (10 weeks). Naked axons with demyelination (arrowheads) are indicated by asterisks. Inset: control image of the spinal cord from the age-matched wild type rat. Axons are normally myelinated. Bar = 1 µm.
doi:10.1371/journal.pgen.1001262.g001

established two independent WTC.DMY-*dmy* lines, expressing each *Mrs2* wild-type cDNA under the control of a cytomegalovirus (CMV) promoter (Figure S2A), and found that all *dmy/dmy* transgenic rats exhibited a completely normal phenotype, with no paralysis of the hind limbs. Histopathological analyses demonstrated that both transgenic lines no longer exhibited any sign of demyelination of the CNS (Figure S2B). In addition, lactic acid levels of the cerebrospinal fluid of transgenic *dmy/dmy* rats had returned to the normal range (Figure S2C). Electron microscopic observations revealed that mitochondria of the oligodendrocytes in transgenic rats were normal in their morphology and number (Figure S2D). These findings confirmed that the molecular changes reported above and observed in the *Mrs2* gene were indeed causative of the *dmy*-mutant phenotypes. For this reason we decided that the symbol of the mutant allele should, from now on, be changed to $Mrs2^{dmy}$.

MRS2-GFP recombinant protein is expressed in the mitochondria

To characterize the tissues and cell types expressing MRS2 as well as the subcellular localization of this protein in the CNS, we generated a strain of rats transgenic for a recombinant MRS2-GFP BAC clone. These transgenic rats were expected to express recombinant protein under the control of the endogenous, normal *Mrs2* promoter. We found that cytoplasmic dot-like MRS2-GFP